

Dormant senescence-prone cells (DSPC): a lifetime memory about systemic genotoxic stress

Katerina Leonova

Roswell Park Comprehensive Cancer Center

Ilya Gitlin

Genome Protection, Inc.

Anatoli Gleiberman

Genome Protection, Inc. <https://orcid.org/0000-0001-8491-0826>

Ilia Toshkov

Genome Protection, Inc.

Nicholas Trageser

Roswell Park Comprehensive Cancer Center

Natalia Issaeva

University of North Carolina

Marina Antoch

Roswell Park Cancer Institute

Andrei Gudkov (✉ andrei.gudkov@roswellpark.org)

Roswell Park Comprehensive Cancer Center <https://orcid.org/0000-0003-2548-0154>

Article

Keywords: radiation, frailty index, longevity, p53, DNA damage response, biodosimetry, tumorigenicity, wound healing, tumor stroma, mesenchymal cell, cell cycle, senescent cell, mesenchymal cell, high fat diet, obesity, life span, dormant senescence-prone cells, senescence-associated secretory phenotype

Posted Date: July 18th, 2022

DOI: <https://doi.org/10.21203/rs.3.rs-1844327/v1>

License:   This work is licensed under a Creative Commons Attribution 4.0 International License.

[Read Full License](#)

Dormant senescence-prone cells (DSPC): a lifetime memory about systemic genotoxic stress

Katerina I. Leonova^{1*}, Ilya I. Gitlin^{2*}, Anatoli S. Gleiberman², Ilia Toshkov², Nicholas H. Trageser¹, Natalia Issaeva³, Marina P. Antoch⁴ and Andrei V. Gudkov^{1,2,5}

¹Department of Cell Stress Biology, Roswell Park Comprehensive Cancer Center, Buffalo, Buffalo, NY14263; ²Genome Protection, Inc., Buffalo, NY; ³Department of Otolaryngology/Head and Neck Surgery, Department of Pathology and Lab Medicine, Lineberger Comprehensive Cancer Center, UNC-Chapel Hill, Chapel Hill, NC 27514, and ⁴Department of Pharmacology and Therapeutics, Roswell Park Comprehensive Cancer Center, Buffalo, NY14263

⁵Corresponding author: andrei.gudkov@roswellpark.org

*Equal contribution first authors.

Short title: Dormant senescence-prone cells and aging

Key words: radiation, frailty index, longevity, p53, DNA damage response, biodosimetry, tumorigenicity, wound healing, tumor stroma, mesenchymal cell, cell cycle, senescent cell, mesenchymal cell, high fat diet, obesity, life span, dormant senescence-prone cells, senescence-associated secretory phenotype.

Abstract

Systemic genotoxic stress is expected to generate senescent cells and accelerate aging. Surprisingly, mice subjected to lethal dose of total body irradiation and rescued by bone marrow transplantation (TBI^{BMT}) showed neither gain of aging-related frailty nor increase in senescence markers. Mesenchymal cells in various tissues of TBI^{BMT} mice do not undergo senescence and stay dormant with unrepaired DNA breaks during the entire life of the animal and activate senescence program only after they are forced into cell divisions *ex vivo* or *in vivo*. Accumulation of such dormant senescence-prone cells (DSPC) has no physiological effects under normal life conditions but is associated with impaired wound healing, decelerated tumor growth due to inefficient scarring and stroma formation and rapid increase in frailty and death after placement on a high-fat diet suggesting the involvement of DSPC accumulation in obesity-induced health decline in cancer survivors following genotoxic treatments.

Introduction

The link between systemic genotoxicity and aging^{1,2,3-5} is the cornerstone of a hypothesis claiming the role of life-long accumulation of irreversibly arrested senescent cells (SenC), resulting from cell response to genotoxic stresses⁶⁻⁹. SenC contribute to pathogenesis of aging presumably by their senescence-associated secretory phenotype (SASP), a continuous release of bioactive factors, which create conditions of chronic systemic inflammation^{10,11}. Rejuvenating effects of “senolytic treatments” leading to eradication of cells with SenC markers support this hypothesis^{12,13} that explains chronological aging as a consequence of translation of endogenous and exogenous genotoxicities into altered tissue microenvironment via DNA damage response and accumulation of pathogenic SenC¹⁴⁻¹⁶.

Cell response to DNA damage is a complex of highly regulated mechanisms acting to reduce the risks to the organism^{17,18}. Depending on the stage of the cell cycle, type of differentiation, the severity of DNA damage and metabolic state cells respond to stress by activating DNA repair, arrest at the cell cycle checkpoints, induction of senescence or apoptosis^{19,20}. With the exception of senescence, other manifestations of DNA damage response are dynamic and relatively short lasting, what reduce their impact on the long-term pathogenic consequences of genotoxicity. Senescence is the predominant type of response to DNA damage of mesenchymal cells²¹⁻²³ suggesting that these cells are major contributors to SenC-associated pathologies.

SenC-based aging paradigm suggests that exposure of mammalian organism to severe genotoxic stress *in vivo* would result in accumulation of SC and accelerated aging. Hence, total body irradiation (TBI) or treatment with DNA damaging chemotherapeutic drugs are expected to accelerate aging^{24,25,26}. In fact, anti-cancer therapy does cause long-term pathological side effects partially resembling aging-associated frailty²⁷, the severity of which can be worsened by obesity in cancer survivors⁵⁶. Here we attempted to create a SenC-driven accelerated aging model using extreme levels of systemic genotoxic stress caused by lethal TBI capable of causing DNA damage in virtually all cells of the mouse. To enable long-term survival, we rescued mice with syngeneic BMT and studied their aging process and SenC dynamics. We found that DNA damage in mesenchymal cells does not lead to the appearance of SenC *in vivo* and persists indefinitely in dormant state without physiological manifestation in the form of dormant senescence-prone cells (DSPC). DSPC turn on senescence program and reveal themselves as pathogens under the conditions that stimulate their proliferation including the induction of adipogenesis.

Results

Severe TBI followed by BMT is not translated into increased frailty index and SenC accumulation in mice

To establish a model of DNA-damage-accelerated aging and to estimate the dynamics of onset of aging phenotype following severe genotoxic stress, we subjected young adult (9-12 weeks old) C57BL/6 male mice to lethal doses (11-13 Gy) of total body irradiation (TBI) followed by bone marrow transplantation (BMT) to prevent lethality (TBI^{BMT} mice). Irradiated and non-irradiated age-matched control animals were monitored for prolonged periods of time, during which representative groups of both kinds were sacrificed for histopathological analysis, *ex vivo* growth of cells from various tissues and estimation of objective physiological age.

To quantitatively assess age-associated decline in physiological functions we utilized physiological frailty index (PFI)²⁸, a cumulative parameter reflecting progressive deviations of physiological, physical and biochemical parameters from their norm during animals' aging (see Materials and Methods). A function of PFI growth of with age can serve as a calibration curve to determine health condition equivalence to certain biological age (**Fig 1A**) and thereby estimate aging-rates in response to various treatments. Contrary to our expectations, we observed a slight but reliable and reproducible decrease in PFI of TBI^{BMT} animals measured in 60-weeks old mice, one year following TBI, indicative of better overall performance of TBI^{BMT} mice vs untreated animals during more than a year following severe systemic genotoxic stress (**Fig. 1B**). Regardless of the unexpected PFI appearance, TBI^{BMT} mice had about 20% shorter average lifespan vs non-irradiated controls (**Fig. 1C**).

Our attempts to find any systemic manifestations of accelerated aging in TBI^{BMT} mice did not reveal any obvious markers of exposure to high dose of TBI: with exception of grey hair, no morphological differences could be detected between among tissues of irradiated and non-irradiated mice up to 98 weeks following TBI (**Supplementary Figure S1**). We also failed to detect differences in the speed or scale of accumulation of cells with SenC markers in tissues of irradiated vs non-irradiated mice as evident from the results of *in situ* SA- β -gal staining of tissues (shown for lungs in **Supplemental Figure S1**) and comparison of the levels of luciferase activity in the mice carrying firefly luciferase reporter gene knocked in the *p16(Ink4a)* gene in their germ line and driven by *p16(Ink4a)* promoter²⁹ (**Fig. 1D**).

Old mammals are known to be prone to systemic inflammation that is recognized as one of the key signs of aging ("inflammaging"³⁰) and is commonly attributed to high risk of age-related diseases³¹. In fact, two-year-old mice differ dramatically from one-year-old animals in the number

and degree of activation of numerous proinflammatory cytokines in response to treatment with TLR4 agonist LPS (**Fig. 1E**). However, TBI^{BMT} mice were much close to the unirradiated control in their responsiveness to LPS treatment than to chronologically aged mice (**Fig. 1E**).

The results of global gene expression profiling are also consistent with the lack of strong aging-accelerating effect of irradiation in TBI^{BMT} mice. As evident from the data analysis presented in **Fig. 1F**, there are 10 times less genes that are differentially expressed in the lungs of untreated and TBI^{BMT} mice than between the lungs of mid-aged and old animals. Moreover, there is only partial overlap between sets of differentially represented transcripts in these two pairs of compared datasets. Hence, TBI^{BMT} mice do not accelerate acquisition of inflammatory gene expression signature typical for old animals (**Supplementary Table S1**).

Undetectable increase in SenC and lack of indications of DNA damage response visible by transcriptome analysis raised the question about the persistence of DNA damage in TBI^{BMT} mice. We used a TUNEL technique capable of revealing persistent post-radiation DNA breaks *in situ*^{57,58}. The results illustrated by **Fig. 1G** and **Supplementary Fig S2** indicate that a proportion of cells in the organs from TBI^{BMT} mice has DNA breaks, while the cells from untreated control animals do not. Remarkably, this proportion remains unchanged in TBI^{BMT} mice throughout the whole period of observation (>12 months) with significantly less pronounced elevation of cells with DNA breaks observed during chronological aging.

All these observations cardinally contradicted our expectations from the physiological consequences of exposure to high TBI doses: we could neither detect accumulation of SenC *in vivo* nor accelerated acquisitions of indicators of aging regardless of the lifetime persistence of DNA damage within studied tissues. This apparent paradox did not have obvious explanation and required in-depth investigation.

Mesenchymal cells in TBI^{BMT} mice retain lifetime commitment to senescence triggered by proliferation stimuli

To characterize properties of cells with persistent DNA damage in tissues we established primary cultures from different organs of TBI^{BMT} mice primarily consisting of cells of mesenchymal origin. Inability to detect accumulation of senescent cells in tissues of TBI^{BMT} mice strikingly contrasted with massive conversion of mesenchymal cells from their organs to senescence upon plating in tissue culture (**Fig. 2A, B, Supplementary Fig. S3**). The proportion of cells with mesenchymal markers that seize proliferation and start expressing “senescence-associated” β -galactosidase activity (SA- β -gal), a marker of SC³² was dependent on the dose of radiation reaching >80% at TBI doses higher than 11 Gy (**Fig. 2C**). Proliferation arrest was accompanied with constitutive

accumulation of phosphorylated histone γ H2AX and reduction in another chromatin protein HMGB1 (**Fig. 2D**), both known to be SenC biomarkers³³. The arrested cells also start secreting cytokines indicative of acquisition of senescence-associated secretory phenotype (SASP)³⁴ (**Fig. 2E**).

As expected, conversion of mesenchymal cells from TBI^{BMT} mice to SC was p53-dependent and not observed in p53-null mice (**Fig. 2B, E**). We concluded that mesenchymal tissue in TBI^{BMT} mice that received more than 11GY TBI predominantly consisted of cells that reside with damaged DNA during the entire mouse life (**Supplementary Fig. S4**) without acquisition of SenC biomarkers but committed to turn on senescence program after they are plated in culture, presumably triggered by entering proliferation. We named them dormant senescence-prone cells (DSPC).

To understand events that precede transition of DSPC in TBI^{BMT} mice to SenC, we compared cell cycle parameters of cell populations in the lungs of TBI^{BMT} and non-irradiated age-matched mice both *in vivo* and following plating in culture. According to DNA content analysis, about 96% of cells derived right from the tissue reside in G0/G1 phase, with no detectable cells in S-phase (**Supplementary Fig. S5**). Consistently, global gene expression analysis revealed minimal differences between irradiated and non-irradiated lungs (**Fig. 1E**). Plating in culture has similar consequences for the cells from the lungs of control and TBI^{BMT} mice: in both cases there is a massive transition of cells into the S-phase that occurs during first hours following plating. However, while cells from non-irradiated mice continued to divide, cells from TBI^{BMT} animals seize proliferation as evident from a dramatic drop in the proportion of cells undergoing DNA-replication detected at 72 hours post plating (**Fig. 3A**). Additionally, EdU incorporation in mesenchymal cells isolated from intact or TBI^{BMT} mice was p53 dependent (**Fig. 3A, bottom panel**).

Conversion to senescence of mesenchymal cells from TBI^{BMT} mice was accompanied with replication stress and constitutive activation of DNA damage response. In contrast to cells isolated from the lungs of non-irradiated age-matched mice, TBI^{BMT} cells displayed typical markers of stalled replication forks (pRPA) and DNA damage response, γ 2AX and 53BP1 foci formation (**Fig. 3B, C** and **Supplementary Fig. S6**). Genotoxic stress remained in the cells from TBI^{BMT} mice throughout the whole period of observation (multiple weeks) (**Fig. 3D**) and its' level was slightly dependent on the dose of irradiation (**Supplementary Fig. S7**), which is typical for SenC that are known to maintain signs of unresolved DNA damage response^{35,36}. Cell population outgrowing from the lung samples of non-irradiated mice also contained cells with manifestations of DNA damage response but in much lower proportion than those from TBI^{BMT} mice, most likely

reflecting background rate of spontaneous DNA damage observed in mouse cells grown in culture with 20% of oxygen³⁷.

We tested whether conversion of DSPC to SenC can be provoked *in vivo* in tissues of TBI^{BMT} mice by stimulation of proliferation similarly to plating in culture. As a proliferation-inducing stimulus, we used sterile wound model that involves injection of a fine suspension of insoluble aluminum hydroxide that is commonly used as an immunoadjuvant³⁸. When injected subcutaneously, it induces formation of a local capsule consisting of mesenchymal cells and various immunocytes - the process that involves local mesenchymal cell proliferation³⁹. Histochemical staining revealed substantially higher proportion of SA- β -gal-positive cells in the vicinity of capsules from TBI^{BMT} vs non-irradiated age-matched control mice (**Supplementary Fig S8**). This suggests that DSPC to SenC conversion observed in culture mimics natural processes occurring *in vivo* under conditions stimulating proliferation (e.g., wound healing).

Conversion of mesenchymal cells to DSPC state contrasted with the behavior of epithelial cells of TBI^{BMT} mice that is evident from continuous proliferation of epithelial tissues *in vivo* and the capability of *in vitro* explanted epithelial cells to divide with no signs of SenC in contrast to mesenchymal cells from the same tissue (demonstrated for liver cells **Supplementary Fig. S9**). Thus, DNA damage caused by systemic genotoxic stress gets resolved in epithelial tissues but retains forever “memorized” in mesenchymal tissue of TBI^{BMT} in the form of DSPC, which are accumulated in a radiation dose-dependent manner.

Wound scarring and tumor stroma formation are impaired in TBI^{BMT} mice

Under normal life conditions, no detectable pathologies develop in TBI^{BMT} mice even though their mesenchymal tissue may consist of up to 100% of DSPC incapable of proliferation upon stimulation (Figure 2 A-B). We hypothesized, that the presence of DSPC can be phenotypically revealed under conditions that provoke entrance of mesenchymal cells into the cell cycle when DNA damage response and senescence programs are activated. Finding such conditions could provide insights into potential health risks associated with systemic genotoxic stresses accompanying cancer treatment by radiation and chemotherapy, which also presumably are associated with DSPC accumulation.

Conditions of mesenchymal cell growth in tissue culture that trigger DSPC to SenC transition are frequently interpreted as an *in vitro* modeling of wound healing, a process that involves local proliferation of mesenchymal cells participating in regeneration of tissue stromal elements and scar formation^{40,41}. We used a mouse model of skin damage – a dermal incision with a 6mm biopsy punch – to compare the dynamics of wound healing in intact and TBI^{BMT} mice.

Fig 4A shows the size of remaining wound area of control and TBI^{BMT} mice measured daily for 20 days. As evident from the presented data, wound healing was significantly delayed in TBI^{BMT} mice relative to non-irradiated controls (**Supplementary Fig. S10**). Even stronger differences were found in the histology of regenerated skin structure: in non-irradiated mice, significant proportion of cells infiltrating the regenerating area is formed by proliferating (Ki67-positive) mesenchymal cells that can be hardly found in the healing wound of TBI^{BMT} mice consistent with the inability of mesenchymal cells in these mice to proliferate (**Fig. 4B**). As a result, wound closure in TBI^{BMT} animals occurs predominantly due to epithelium proliferation and migration with minor mesenchymal involvement in a scar formation. Given established role of SenC as contributors to wound healing⁴², we concluded that even an excessive appearance of SenC in the wounded skin areas could not overbalance the deficiency in mesenchymal precursors capable of proliferation in TBI^{BMT} mice.

Formation of stroma, an essential component of any solid tumor, resembles the process of wound healing and involves proliferating mesenchymal cell⁴³. We, therefore, compared growth of tumors originating from syngeneic melanoma cells, B16, implanted subcutaneously in intact and TBI^{BMT} C57Bl/6 mice that received 11 Gy of TBI 4-6 months prior to tumor cell implantation. TBI of mice with sublethal doses of radiation (which turn only a fraction of mesenchymal cells into the DSPC state) is commonly used for suppression of innate immunity to facilitate engraftment of transplanted tumors. In contrast, mice that received 11 Gy of TBI, the dose that converts the majority of mesenchymal cells into DSPC, resulted in a strong delay of tumor growth (**Fig. 5A-C**). The majority of transplanted tumors seized growth for weeks after they reached 2-3 mm in diameter, the size above which tumor growth presumably becomes dependent on stroma formation. Histological analysis of subcutaneously grown tumors of equal size revealed dramatic structural differences between tumors of unirradiated vs those of TBI^{BMT} mice: regardless of the similarity in the proportion of proliferating cells, tumors of TBI^{BMT} mice contained massive areas of necrosis consistent with the deficit in stromagenic precursors in irradiated animals (**Fig. 5B**).

Revealing and suppressing systemic pathogenic potential of DSPC accumulation

The absence of obvious pathologies in adult TBI^{BMT} mice is likely explained by the lack of DNA damage processing and entrance into senescence program of non-proliferating mesenchymal cells. If true, then one would expect different remote consequences of TBI+BMT in growing young TBI^{BMT} animals which have actively proliferating mesenchymal cells. In fact, BMT prolonged life of C57BL/6 mice, which received 10Gy TBI at 4 weeks of age, for only 6 weeks, while similar

procedure applied to adult animals extended their life to 100 weeks (if they are maintained on a healthy diet) (**Fig. 6A**).

To reveal pathologic consequences of induced systemic proliferation of mesenchymal cells in TBI^{BMT} mice we chose the induction of obesity as a naturally occurring physiological condition that involves massive conversion of mesenchymal stem cells (MSCs) to preadipocytes, a process that includes cell proliferation⁵⁹. C57BI/6 mice were placed on a high fat diet leading to gradual weight gain, accelerated growth of PFI and reduced longevity of non-irradiated mice by about 25% as compared to mice on a healthy diet (similar reduction in lifespan was observed in TBI^{BMT} mice on a regular diet). Remarkably, a high fat diet had a dramatically stronger negative health effect in TBI^{BMT} reducing their lifespan, on average, by 60 weeks from 100 to 40 weeks (**Fig. 6B**). They also showed significantly less pronounced weight gain than their age-matched non-irradiated controls presumably due to the deficit of mesenchymal precursors capable of proliferation and essential for growing adipose tissue (**Supplementary Fig. S11**). Consistently, PFI of TBI^{BMT} mice rapidly grew until their death occurring, on average, within 24 weeks following placement on the obesity-provoking diet (**Fig. 6C**).

Thus, massive accumulation of DSPC in adult TBI^{BMT} mice, being benign and dormant under normal life conditions, is accompanied with a severe systemic pathology consistent with premature aging under condition that triggers proliferation of DSPC (the induction of obesity) suggesting a causative relationship between the two. Cardinal difference in consequences of TBI+BMT for growing and adult mice to is consistent with this explanation. The observed phenomenon resembles and provides plausible mechanistic explanation for a systemic health decline frequently associated with obesity in cancer survivors that underwent systemic genotoxic therapies⁵⁶.

Discussion

Our observations indicate that even most severe systemic genotoxicity, which results in DNA damage occurring in virtually every cell, is not necessarily translated into accumulation of SC and aging acceleration. Accumulated DNA damage either become fully resolved (i.e., in epithelial cells of tissues with rapid cell turnover) or stay hidden (in nonproliferating mesenchymal cells) throughout the entire life. This striking counterintuitive result may reflect unnaturally clean challenge-free conditions of modern animal facilities, which, however, are not too far from the conditions of human life in civilized societies.

Cumulative genotoxicity memorized in the form of DSPC has a chance to be phenotypically revealed under conditions when DSPC are forced into the cell cycle. Specific

phenotypic manifestation of DNA damage depends on the scale and stimulus of DSPC → SC transition. Local effects involve impaired wound healing and inhibition of stromagenesis suppressing tumors growth. Systemic engagement of DSPC in proliferation stimulated by obesity-inducing diet can be translated into universal pathologies resembling accelerated aging. The diversity of responses demonstrates how conditions of life following exposure to genotoxic treatments, specifically avoidance of provoking massive conversion of DSPC→SC, can influence health and longevity. Our observations provide plausible explanation and likely mimics systemic health decline frequently occurring in breast cancer survivors who gained weight following successful recovery from cancer treatment⁴⁴. Although fewer studies address weight changes and survival following cancer treatment, it has been eluded that in breast cancer survivors weight gain after diagnosis leads to increased breast cancer recurrence and mortality⁴⁵⁻⁴⁷.

Lack of guaranteed translation of systemic genotoxic stress into accelerated aging indicates that aging development resembles the two-stage process as chemical carcinogenesis⁴⁸ that also involves: (i) initiation – massive accumulation of cells predisposed to senescence, who not yet acquired fully developed senescent phenotype, and (ii) promotion stages – exposure to conditions that reveal senescence-prone capabilities of “initiated” pre-senescent DSPC by pushing them into proliferation and formation of a massive pool of SC followed by acceleration of aging. “Initiated” senescence-prone cells can stay in the organism indefinitely, thus memorizing individual life history of genotoxicity and determining the speed of aging development under conditions favoring the promotion of dormant senescence-prone cells to *bone fide* senescence state.

Accumulation of DSPC, being a function of cumulative genotoxicity, opens a potential approach to biodosimetry, a long wanted but still poorly addressed clinical need⁴⁹. Another potential opportunity involves development a pharmacological agent capable of “discharging” DSPC by activation of DNA repair in them as it happens in epithelial cells, which could be considered for prophylaxis of accelerated aging in victims of genotoxic stresses. Both today remain theoretical possibilities with no obvious practical solutions.

DSPC phenomenon broadens the list of outcomes of DNA damage at cellular level, which formerly included (i) reversible growth arrest at one of the cell cycle checkpoints (a property of the majority of epithelial cells), (ii) apoptosis (common response of the majority of hematopoietic and some epithelial cells) and (iii) senescence (typical for mesenchymal cells in culture and melanocytes in vitro and in vivo). We can now add to them (iv) dormant senescent-prone state, a common situation with mesenchymal cells that fail to process DNA damage in vivo unless they

are forced to enter the cell cycle. Whether the DSPC phenomenon is limited to mesenchymal cells or involves cells of other epigenetic niches (i.e. endothelium or glia) remains unknown.

We also do not have mechanistic explanation for obvious tissue specific differences in control of DNA damage response determining one of four alternative cell fates following DNA damage. Lack of attempts to resolve DNA damage by mesenchymal cells *in vivo* may reflect a tight regulation between DNA repair and the cell cycle and, specifically, temporal silencing of the major DNA damage repair mechanisms at G0, as well as impeded DNA damage resolution when these cells begin proliferation (Ambrosio et al, Oncotarget 2015)⁶². In fact, the decision of which repair system to use depends on both, the type of lesion and on the cell-cycle phase of the cell, and although there is some evidence of checkpoint arrests to DNA damage in quiescent cells⁵⁰, most checkpoints and some repair mechanisms operate in cycling cells. Cells in G1 are responsible to repair accidental damage, such as damage from UV, chemical agents or ionizing irradiation, before the onset of replication. Double-stranded breaks (DSBs) are typically repaired in G1 by mechanism of non-homologous end joining (NHEJ) and by homologous recombination (HR) in S-phase^{26,51,52}.

Lack of DNA damage resolution by DSPC may have important though still elusive biological sense. It may, for example, be a mechanism protecting adult organisms from pathological consequences of massive accumulation of SC that can be translated into accelerated premature aging and increased risk of age-related diseases. If true, then growing organism of a child, which has a significant proportion of mesenchymal cells in proliferating state, seems to be much more vulnerable to delayed consequences of systemic genotoxicity since it allows easier translation of DNA damage into pathologies associated with accumulation of SC: accelerated aging and age-related diseases⁵³. This consideration is supported by a growing body of evidence demonstrating reduced longevity, earlier acquisition and higher frequency of metabolic and neoplastic diseases among survivors of childhood malignancies who underwent severe genotoxic treatments⁵⁴. Similar situation occurs in adult cancer survivors who gain weight due to stimulated adipogenesis (see above). Both categories of patients are expected to benefit from development of a DSPC-discharging and SC-eradicating therapies.

ACKNOWLEDGMENTS

We thank Patricia Stanhope-Baker for help with manuscript editing and staff of Laboratory Animal Shared Resources (Roswell Park) for help with animal care.

Funding:

Genome Protection, Inc. (AVG)

Roswell Park Alliance Foundation (AVG)

Author contributions:

Basic observation: KIL

Conceptualization: AVG, KIL, IIG

Methodology: KIL, IIG, MPA, NI

Investigation: KIL, IIG, MPA, ASG, NI, IT, NHT

Funding acquisition: AVG

Project administration: AVG, KIL

Manuscript writing: AVG, KIL, IIG

Manuscript editing: MPA, NI

Competing interests:

Authors declare that they have no competing interests.

Data and materials availability:

All data and materials generated within this study and used in the analysis will be provided to any researcher for purposes of reproducing or extending the analysis under materials transfer agreements (MTAs). All data are available in the main text or the supplementary materials.

References

1. Schumacher, B., Garinis, G. A. & Hoeijmakers, J. H. J. Age to survive: DNA damage and aging. *Trends Genet.* **24**, 77–85 (2008).
2. Hoeijmakers, J. H. DNA damage, aging, and cancer. *N Engl J Med* **361**, 1475–1485 (2009).
3. Jackson, S. P. & Bartek, J. The DNA-damage response in human biology and disease. *Nature* **461**, 1071–1078 (2010).
4. de Boer, J. *et al.* Premature aging in mice deficient in DNA repair and transcription. *Science* **296**, 1276–1279 (2002).
5. Lehmann, A. R. DNA repair-deficient diseases, xeroderma pigmentosum, Cockayne syndrome and trichothiodystrophy. *Biochimie* **85**, 1101–1111 (2003).
6. Rubio, M. A., Davalos, A. R. & Campisi, J. Telomere length mediates the effects of telomerase on the cellular response to genotoxic stress. *Exp. Cell Res.* **298**, 17–27 (2004).
7. Campisi, J. Senescent cells, tumor suppression, and organismal aging: Good citizens, bad neighbors. *Cell* **120**, 513–522 (2005).
8. Seluanov, A. *et al.* Change of the Death Pathway in Senescent Human Fibroblasts in Response to DNA Damage Is Caused by an Inability To Change of the Death Pathway in Senescent Human Fibroblasts in Response to DNA Damage Is Caused by an Inability To Stabilize p53. *Mol. Cell. Biol.* **21**, 1552–1564 (2001).
9. Herbig, U., Jobling, W. A., Chen, B. P. C., Chen, D. J. & Sedivy, J. M. Telomere shortening triggers senescence of human cells through a pathway involving ATM, p53, and p21CIP1, but not p16INK4a. *Mol. Cell* **14**, 501–513 (2004).
10. Rodier, F. *et al.* Persistent DNA damage signalling triggers senescence-associated inflammatory cytokine secretion. *Nat. Cell Biol.* **11**, 973–979 (2009).
11. Salminen, A., Kauppinen, A. & Kaarniranta, K. Emerging role of NF-κB signaling in the induction of senescence-associated secretory phenotype (SASP). *Cell. Signal.* **24**, 835–845 (2012).

12. Baker, D. J. *et al.* Clearance of p16Ink4a-positive senescent cells delays ageing-associated disorders. *Nature* **479**, 232–6 (2011).
13. Baker, D. J. *et al.* Naturally occurring p16 Ink4a -positive cells shorten healthy lifespan. *Nature* **530**, 1–5 (2016).
14. Krtolica, A., Parrinello, S., Lockett, S., Desprez, P. Y. & Campisi, J. Senescent fibroblasts promote epithelial cell growth and tumorigenesis: a link between cancer and aging. *Proc. Natl. Acad. Sci. U. S. A.* **98**, 12072–7 (2001).
15. Burhans, W. C. & Weinberger, M. DNA replication stress, genome instability and aging. *Nucleic Acids Res.* **35**, 7545–7556 (2007).
16. Herbig, U., Ferreira, M., Condel, L., Carey, D. & Sedivy, J. M. Cellular Senescence in Aging Primates. *Science (80-.).* **311**, 1–2 (2006).
17. Zhou, B. S. & Elledge, S. J. Checkpoints in perspective. *Nature* **408**, 433–439 (2000).
18. Kastan, M., Onyekwere, O., Sidransky, D., Vogelstein, B. & Craig, R. Participation of p53 protein in the cellular response to DNA damage. *Cancer Res* **51**, 6304–6311 (1991).
19. Gandarillas, A. Epidermal differentiation, apoptosis, and senescence: Common pathways? *Exp. Gerontol.* **35**, 53–62 (2000).
20. Chen, Q. M., Liu, J. & Merrett, J. B. Apoptosis or senescence-like growth arrest: influence of cell-cycle position, p53, p21 and bax in H2O2 response of normal human fibroblasts. *Biochem. J.* **347**, 543–51 (2000).
21. Fehrer, C. & Lepperdinger, G. Mesenchymal stem cell aging. *Exp. Gerontol.* **40**, 926–930 (2005).
22. Goldstein, S. Replicative Senescence: The Human Fibroblast Comes of Age. *Science*, **249**, 1129–1133 (1990).
23. Zhu, J., Woods, D., McMahon, M. & Bishop, J. M. Senescence of human fibroblasts induced by oncogenic Raf. *Genes Dev.* **12**, 2997–3007 (1998).
24. Collado, M., Blasco, M. A. & Serrano, M. Cellular Senescence in Cancer and Aging. *Cell* **130**, 223–233 (2007).

25. Campisi, J. & d'Adda di Fagagna, F. Cellular senescence: when bad things happen to good cells. *Nat. Rev. Mol. Cell Biol.* **8**, 729–740 (2007).
26. Garinis, G. A., Van Der Horst, G. T. J., Vijg, J. & Hoeijmakers, J. H. J. DNA damage and ageing: new-age ideas for an age-old problem. *Nat. Cell Biol. cell Biol.* **10**, 1241–1247 (2008).
27. Burtner, C. R. & Kennedy, B. K. Progeria syndromes and ageing: what is the connection? *Nat. Rev. Mol. Cell Biol.* **11**, 567–578 (2010).
28. Antoch M. P. *et al.* Physiological frailty index (PFI): quantitative in-life estimate of individual biological age in mice. *Aging (Albany NY)* **9**, 615-626 (2017).
29. Burd, C. E. *et al.* Monitoring tumorigenesis and senescence in vivo with a p16 INK4a-luciferase model. *Cell* **152**, 340–351 (2013).
30. Franceschi, C. *et al.* Inflammaging and anti-inflammaging: A systemic perspective on aging and longevity emerged from studies in humans. *Mech. Ageing Dev.* **128**, 92–105 (2007).
31. Franceschi, C. & Campisi, J. Chronic inflammation (Inflammaging) and its potential contribution to age-associated diseases. *Journals Gerontol. - Ser. A Biol. Sci. Med. Sci.* **69**, S4–S9 (2014).
32. Itahana, K., Campisi, J. & Dimri, G. P. Methods to detect biomarkers of cellular senescence: The senescence-associated β -galactosidase assay. *Methods Mol. Biol.* **371**, 21–31 (2007).
33. Davalos, A. R. *et al.* p53-dependent release of Alarmin HMGB1 is a central mediator of senescent phenotypes. *J. Cell Biol.* **201**, 613–629 (2013).
34. Coppé, J. P. *et al.* A human-like senescence-associated secretory phenotype is conserved in mouse cells dependent on physiological oxygen. *PLoS One* **5**, (2010).
35. Campisi, J. Aging, Cellular Senescence, and Cancer. *Annu. Rev. Physiol.* **75**, 685–705 (2013).
36. Rodier, F. *et al.* DNA-SCARS: distinct nuclear structures that sustain damage-induced senescence growth arrest and inflammatory cytokine secretion. *J. Cell Sci.* **124**, 68–81

- (2011).
37. Parrinello, S. *et al.* Oxygen sensitivity severely limits the replicative lifespan of murine fibroblasts. *Nat. Cell Biol.* **5**, 741–747 (2003).
 38. Baylor, N. W., Egan, W. & Richman, P. Aluminum salts in vaccines--US perspective. *Vaccine* **20 Suppl 3**, S18-23 (2002).
 39. Valtulini, S. *et al.* Aluminium hydroxide-induced granulomas in pigs. *Vaccine* **23**, 3999–4004 (2005).
 40. Gurtner, G., Werner, S., Barrandon, Y. & Longaker, M. Wound repair and regeneration. *Nature* **453**, 314–321 (2008).
 41. Wu, Y., Chen, L., Scott, P. G. & Tredget, E. E. Mesenchymal stem cells enhance wound healing through differentiation and angiogenesis. *Stem Cells* **25**, 2648–2659 (2007).
 42. Demaria, M. *et al.* An essential role for senescent cells in optimal wound healing through secretion of PDGF-AA. *Dev. Cell* **31**, 722–733 (2014).
 43. Kalluri, R. & Zeisberg, M. Fibroblasts in cancer. *Nat. Rev. Cancer* **6**, 392–401 (2006).
 44. Irwin, M. L. *et al.* Changes in body fat and weight after a breast cancer diagnosis: Influence of demographic, prognostic, and lifestyle factors. *J. Clin. Oncol.* **23**, 774–782 (2005).
 45. Holmes, M. D., Chen, W. Y., Feskanich, D., Kroenke, C. H. & Colditz, G. A. After Breast Cancer Diagnosis. *J. Am. Med. Association* **293**, 2479–2486 (2005).
 46. Kroenke, C. H., Chen, W. Y., Rosner, B. & Holmes, M. D. Weight, weight gain, and survival after breast cancer diagnosis. *J. Clin. Oncol.* **23**, 1370–1378 (2005).
 47. Fine, J. T. *et al.* A prospective study of weight change and health-related quality of life in women. *J. Am. Med. Assoc.* **282**, 2136–2142 (1999).
 48. Abel, E. L., Angel, J. M., Kiguchi, K. & DiGiovanni, J. Multi-stage chemical carcinogenesis in mouse skin: fundamentals and applications. *Nat. Protoc.* **4**, 1350–62 (2009).
 49. Swartz, H. M. *et al.* A critical assessment of biodosimetry methods for large-scale incidents. *Health Phys.* **98**, 95–108 (2010).

50. Lukas, C. *et al.* DNA damage-activated kinase Chk2 is independent of proliferation or differentiation yet correlates with tissue biology. *Cancer Res.* **61**, 4990–4993 (2001).
51. Brnzei, D. & Foiani, M. Regulation of DNA repair throughout the cell cycle. *Nat. Rev. Mol. Cell Biol.* **9**, 297–308 (2008).
52. Dasika, G. K. *et al.* DNA damage-induced cell cycle checkpoints and DNA strand break repair in development and tumorigenesis. *Oncogene* **18**, 7883–99 (1999).
53. Childs, B. G., Durik, M., Baker, D. J. & van Deursen, J. M. Cellular senescence in aging and age-related disease: from mechanisms to therapy. *Nat. Med.* **21**, 1424 (2015).
54. Ness, K. K. *et al.* Frailty in childhood cancer survivors. *Cancer* **121**, 1540–1547 (2015).
57. Sharma R., Ahmad G., Esteves S. C., Agarwal A. Terminal deoxynucleotidyl transferase dUTP nick end labeling (TUNEL) assay using bench top flow cytometer for evaluation of sperm DNA fragmentation in fertility laboratories: protocol, reference values, and quality control. *J Assist Reprod Genet.* **33**, 291-300 (2016).
58. Mirzayans R., Murray D. Do TUNEL and Other Apoptosis Assays Detect Cell Death in Preclinical Studies? *Int J Mol Sci.* **21**, 9090 (2020).
59. Tang Q. Q., Lane M. D. Adipogenesis: from stem cell to adipocyte. *Annu Rev Biochem.* **81**, 715-736 (2012).

Legends to Figures

Figure 1. Systemic DNA damage is a poor accelerator of aging. (A) Age-related changes in PFI in male C57BL6 mice (n=7-10/group). PFI indices measured as described using 11 parameters. Data is presented as mean \pm SEM. One-way ANOVA detects significant effect of age on PFI value. (B) PFI of intact and TBI^{BMT} C57BL6 male mice (n=7/group) measured at 52 weeks of age. TBI^{BMT} mice show significant reduction in frailty compared to age-matched controls. (C) C57BL/6 mouse survival data of control versus 11Gy total body irradiation followed by bone marrow transplantation rescue the following day (unpaired t test p value = 0.0039). (D) Age-related induction of p16^{Ink4a} *in vivo* is not accelerated with irradiation. p16^{Ink4a}-promoter-driver luciferase activity was measured at 14 weeks, 35 weeks and 60 weeks after irradiation or in non-irradiated age-matched control. Bioluminescent signal accumulation in a cohort of chronologically aged intact and TBI^{BMT} harboring a hemizygous p16(INK4a) knock-in of luciferase (p16^{LUC} mice; p16^{Ink4a/Luc}) is calculated as whole-body luminescence (total flux; p/s). (E) Comparison of endogenous p16 activity via luciferase in intact young (40 weeks), intact old (98 weeks) and TBI^{BMT} (12 weeks after TBI) mice. Luciferase reporter activity was detected in intact old (98 weeks) mice, but not in TBI^{BMT} or age-matched non-irradiated control. Additionally, the degree of activation of pro-inflammatory cytokines 5 hours after the injection with LPS (10 μ g/mouse) is significantly higher in mice 98 weeks of age than in TBI^{BMT} or non-irradiated age-matched controls. (F) Global gene expression of profile of lung tissue isolated from intact young (40 weeks), intact old (98 weeks) and TBI^{BMT} (40 weeks) mice. (G) TUNEL staining of 40 weeks intact mice, 96 weeks intact mice and 40 weeks TBI^{BMT} mice revealed a greater number of cells with damaged DNA in TBI^{BMT} lung samples than intact mice at either 40 or 96 weeks of age.

Figure 2. Mesenchymal cells isolated from TBI^{BMT} mice are committed to enter senescence *in vitro*. (A) Cells isolated from lung tissues of TBI^{BMT} mice fail to divide *in vitro* and this effect is persistent for many weeks following TBI. (B) Population doubling assessed in cell isolated from intact and irradiated C57BL/6 mice. (C) Lung fibroblasts isolated from TBI^{BMT} mice when plated *in vitro* express senescence associated β -galactosidase activity in irradiation dose-dependent manner. (D) Cytokine level of IL-6 (top) and CXCL-1 (bottom) in the conditioned medium of proliferating (LF) and senescent (LF^{TBI}) lung fibroblasts isolated from intact and irradiated p53 wild-type and p53null mice.

Figure 3. Mesenchymal cells isolated from TBI^{BMT} exhibit DNA damage response. (A-B) Proliferation of cells measured by EdU incorporation of intact and TBI^{BMT} mice analyzed at 8 hours

and 72 hours after plating isolated from p53 wild type and p53 null mice. (C-E) DNA damage in cells plated from TBI^{BMT} mice as demonstrated with γ H2AX and 53BP1 foci formation. Cells with more than 10 foci/nuclear were counted as positive; at least 100 cells were evaluated in two different fields. (F) Cells plated from TBI^{BMT} mice retain DNA damage as detected with γ H2AX and 53BP1 foci formation up to 35 days of being in culture. Cells with more than 10 foci/nuclear were counted as positive; at least 100 cells were evaluated in two different fields.

Figure 4. Deceleration of wound healing process in TBI^{BMT} mice. (A) Two full-thickness excisional wounds were created in the skin of non-irradiated and TBI^{BMT} C57Bl/6 mouse using 6-mm biopsy tool. Wounds were photographed every two days after wounding. Quantification of wound closure from photographs. Three mice per group were followed for 20 days. TBI^{BMT} wounds were delayed in closure starting at day 6 (*P* value at days 6-12<0.001). Data are expressed a percent of the initial wound are. (B) Immunohistochemical analysis of wound site at 10 days after wounding showed a decrease of Ki67 positive cells in the wounds formed in mice after TBI^{BMT}.

Figure 5. Impaired tumor growth in TBI^{BMT} mice. (A) B16F10 subcutaneous tumor growth in TBI^{BMT} and non-irradiated age-matched control C57Bl/6 mice. Mice (n=9) were inoculated subcutaneously with 1.5×10^5 B16F10 cells on a dorsal flank. Palpable tumors were measured daily, and relative volume and tumor free survival was determined. Subcutaneous B16F10 tumors grew significantly slower in TBI^{BMT} mice comparing to age-matched non-irradiated control. (B) Subcutaneously grown B16F10 tumors in C57BL/6 TBI^{BMT} and non-irradiated controls were excised once they reached volume of 200mm³ (n=4). The morphology of these tumors was analyzed with Giemsa staining. More pronounced necrosis visible in the neoplastic nodules of TBI^{BMT} mice than those grown in non-irradiated control. (Blue arrows-neoplastic cells with well-preserved cytoplasmic basophilia; black arrows-areas with necrotic tumor cells; red arrows-infiltrative cells in the surrounding edematous derma). (C) Survival of non-irradiated and TBI^{BMT} B16F10 tumor burden mice was measured. The mean survival of TBI^{BMT} mice was 35.2 days and the mean survival for non-irradiated control was 11.9 days (p value<0.001).

Figure 6. Revealing DSPC-associated phenotype in TBI^{BMT} mice. (A) Sensitivity of 4-week-old C57BL/6 mice to 10Gy of irradiation with bone marrow transplantation. (B) For TBI^{BMT} mice irradiation occurred at 12 weeks of age for adult group. Non-irradiated and TBI^{BMT} adult mice were divided into two groups and placed on either high-fat diet (HFD) or regular diet (RD) (at 16 weeks of age). The survival of these mice was monitored. TBI^{BMT} animals of HFD had a significantly shorter survival than those on normal diet or non-irradiated on either diet. (C) Feeding HFD

increase frailty in TBI^{BMT} mice. Non-irradiated and TBI^{BMT} mice were placed on HFD or RD at 16 weeks of age. PFI was measured at 34 weeks of age.

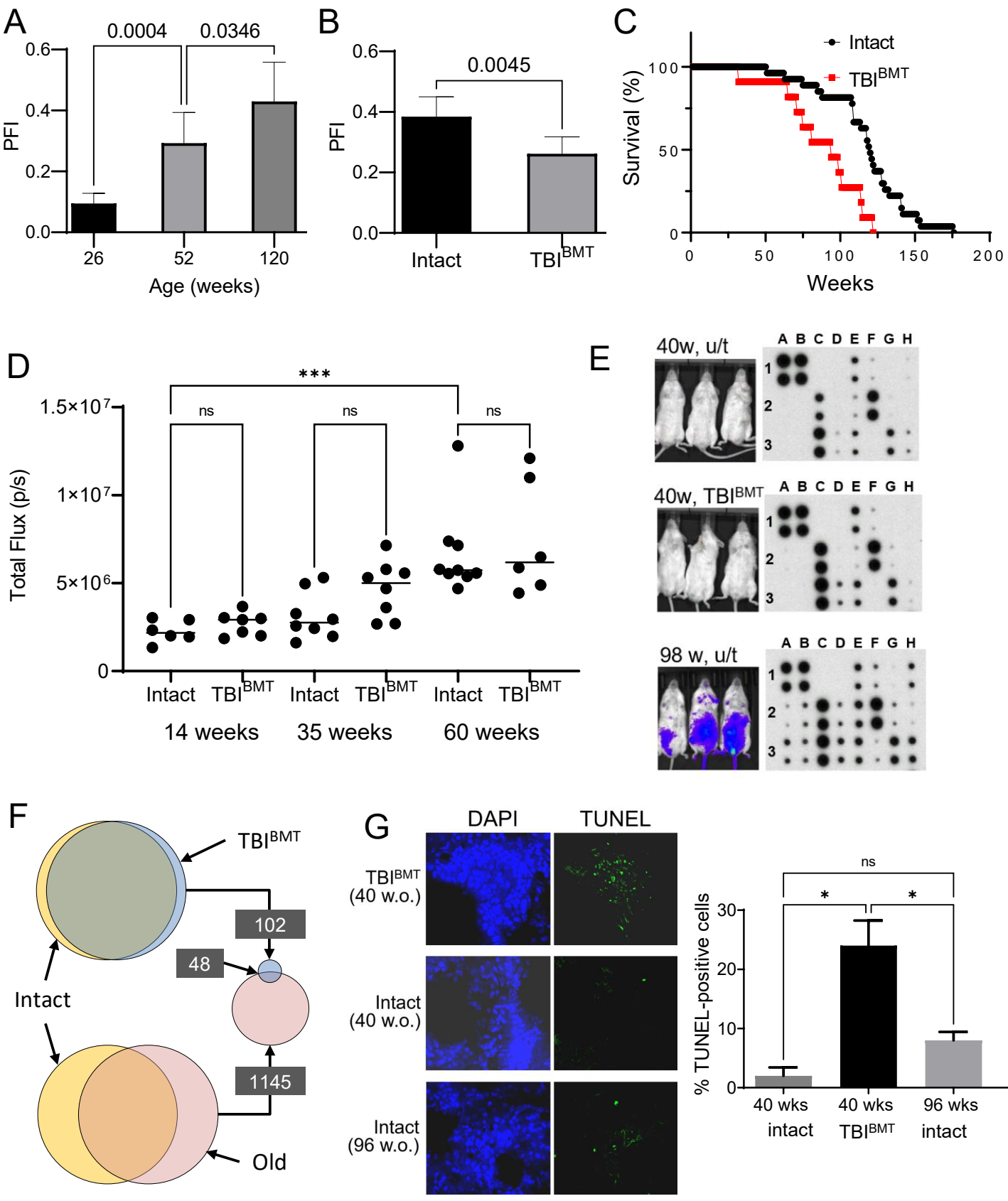


Figure 1

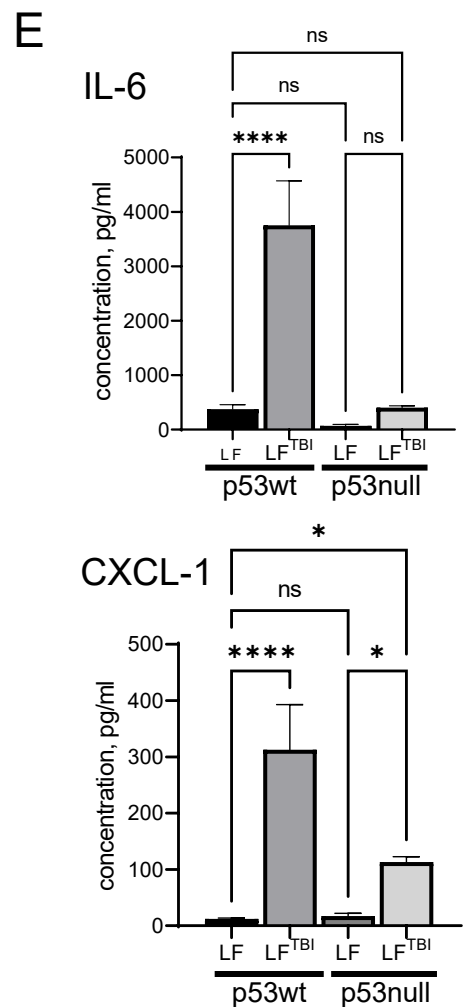
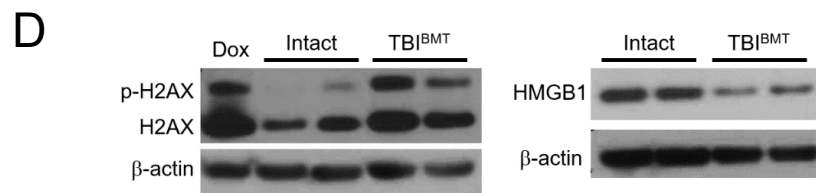
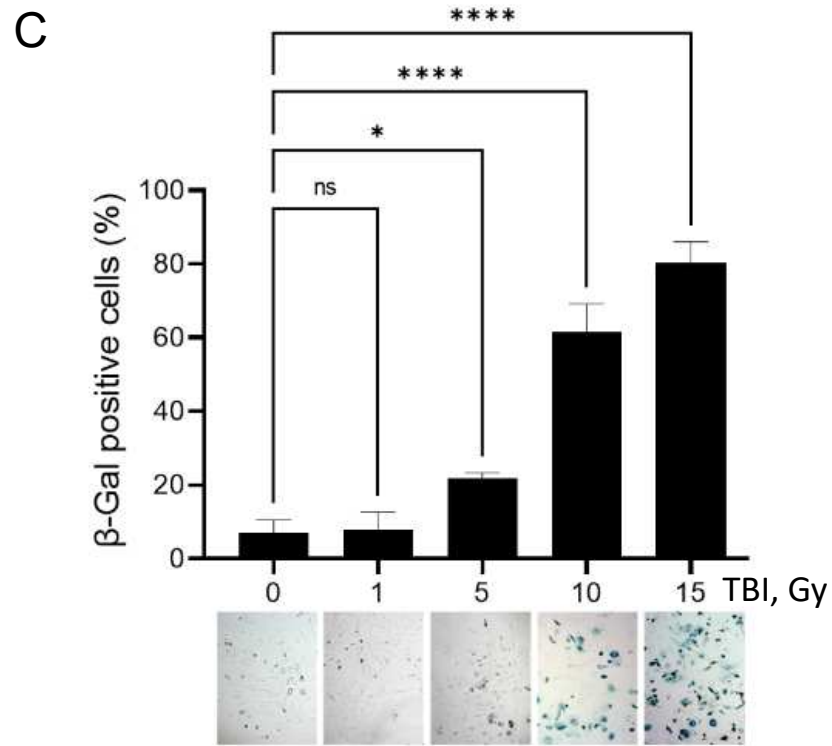
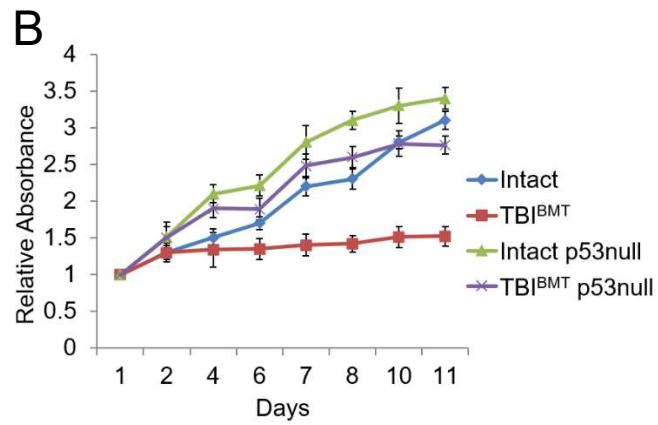
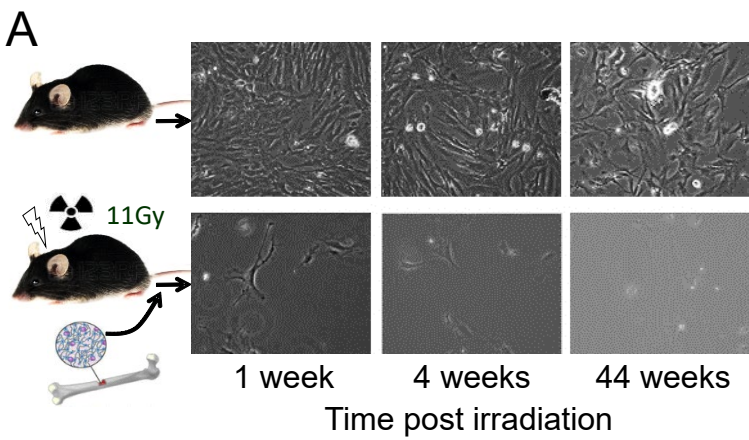


Figure 2

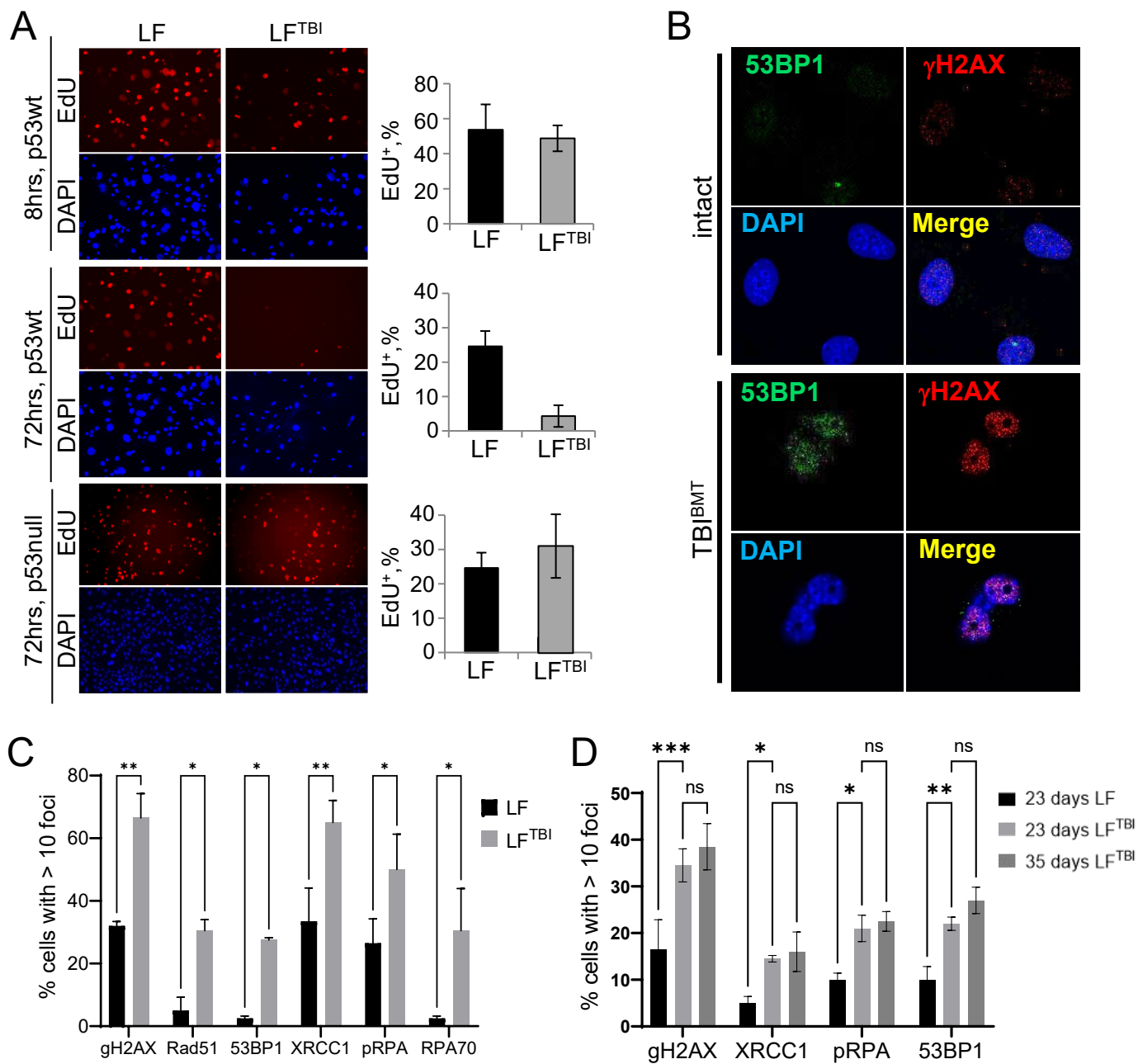


Figure 3

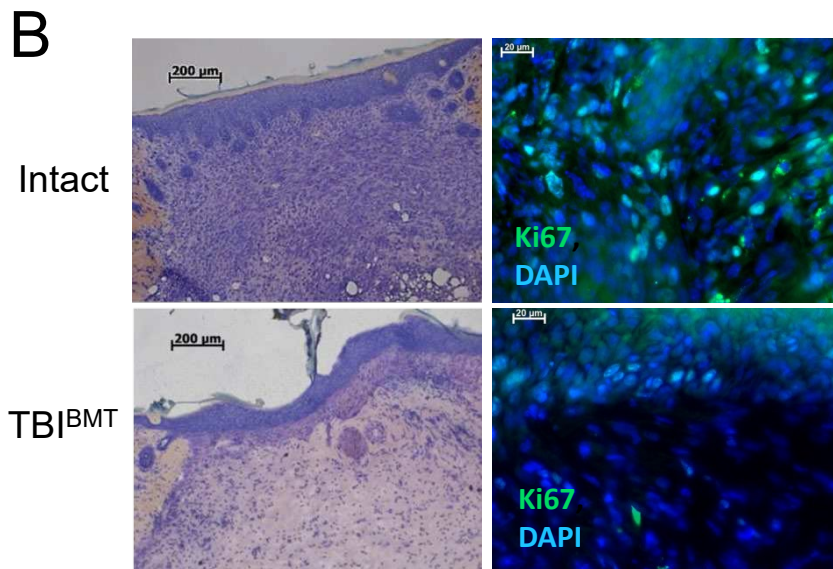
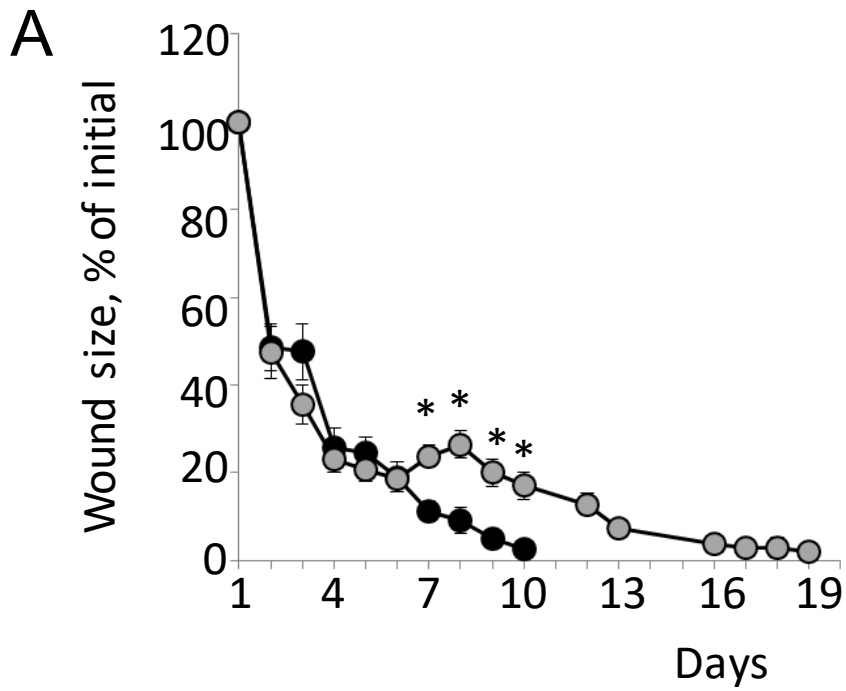


Figure 4

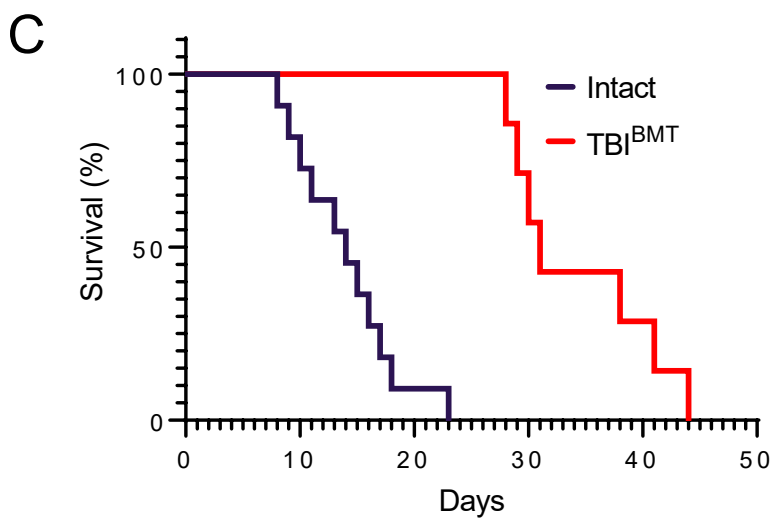
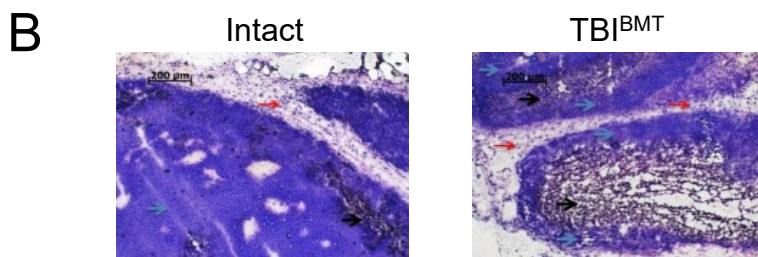
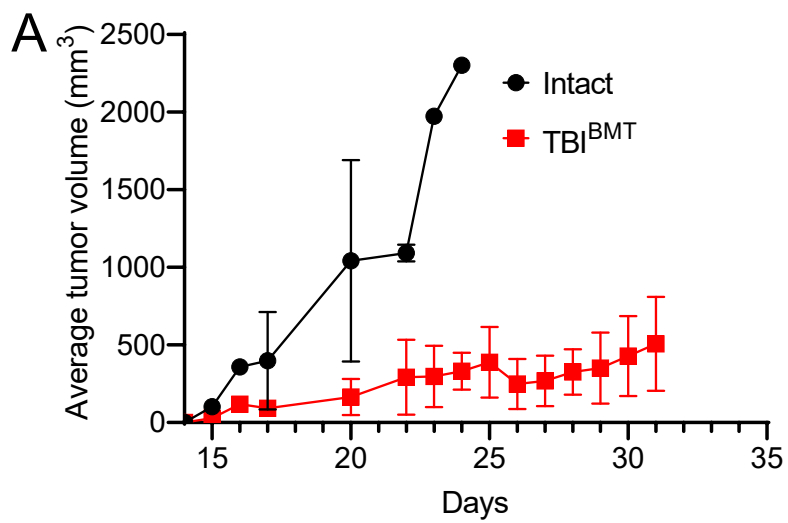


Figure 5

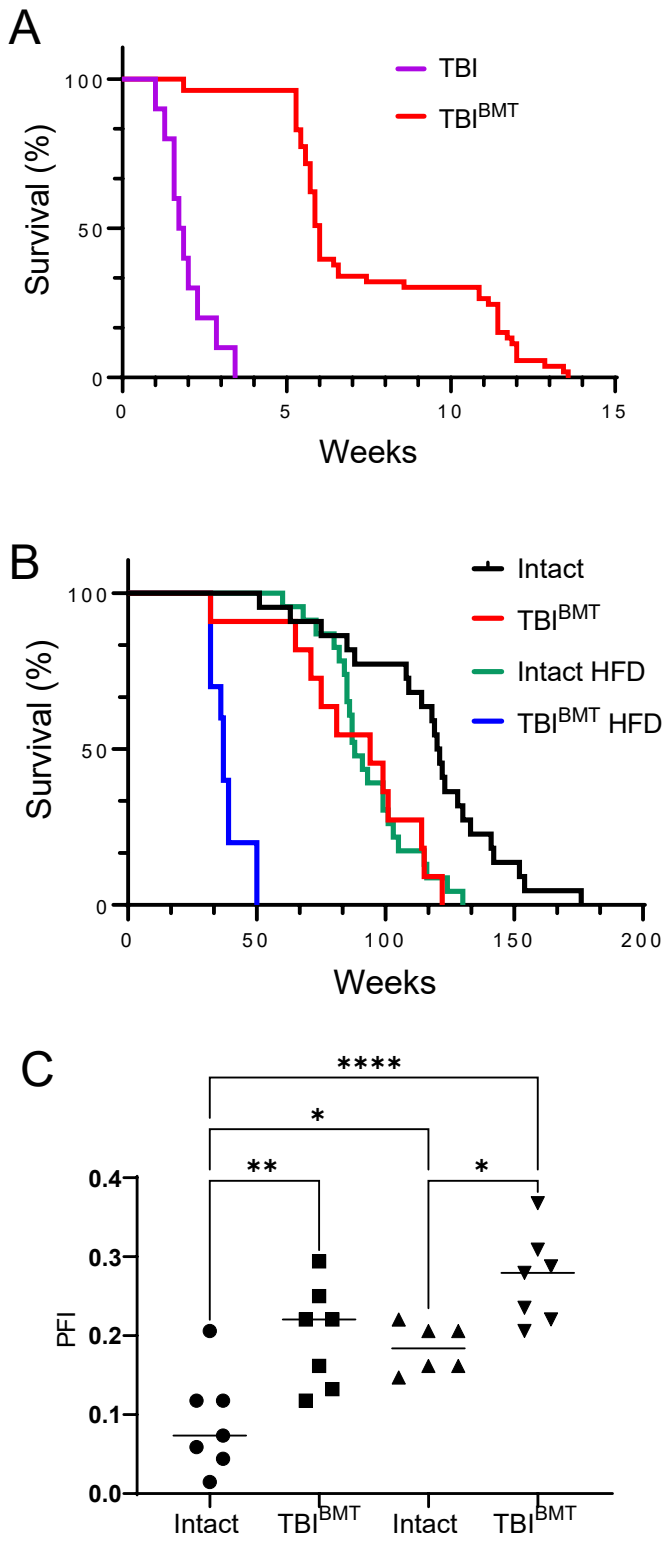


Figure 6

Material and Methods

Mice

All procedures used in this study followed the Public Health Service Policy and the methods and protocols used were approved by the Institutional Animal Care and Use Committee. Male C57BL/6 mice were purchased from Charles River. A colony of p53 wild-type and p53-knockout mice on a C57BL/6 background was maintained by crossing p53^{+/-} females with p53^{-/-} males (purchased from Jackson Laboratories, Bar Harbor, ME) followed by PCR based genotyping of the progeny. p16^{INK4a}-luciferase mice were a kind gift from the laboratory of Dr. Norman E. Sharpless.

Preparation of TBI^{BMT} mice

All mice in the experiments were used at 12 weeks of age, unless specified in the text. Male C57BL/6 mice (12 weeks of age) were irradiated (IR) at various doses specified in the text, total body irradiation (TBI) and were rescued by bone marrow transplantation (BMT) 24 hours after irradiation. Briefly, experimental C57BL/6 mice received a single lethal dose of total body gamma-radiation (TBI^{BMT}). Non-IR donor C57BL/6 mice were used to extract bone marrow suspension by crushing and washing the femurs and tibiae with PBS. Single-cell suspensions were prepared by passing the cells through 30- μ m nylon gauze. Irradiated recipients were reconstituted 24 hours later with approximately 1.0×10^6 bone marrow cells by intravenous injection into the tail vein.

Physiological Frailty Index (PFI) measured parameters

Grip strength measurement: fore limb grip strength measurements were performed using Animal Grip Strength System (San Diego Instruments). Five measurements were recorded for each individual animal and the average value was assigned.

Non-invasive measurement of hemodynamic parameters was performed using CODA apparatus (Kent Scientific) according to manufacturer's protocol. Mice were placed into cylinder-shaped restraint devices and allowed to acclimate for 5 min on a heating platform before blood pressure measurements begin. Body temperature was continuously monitored by observation of animal behavior, tail blood volume and an infrared thermometer. Recorded hemodynamic parameters include systolic, diastolic and mean blood pressure, heart rate, tail blood flow and tail blood volume.

Blood samples collection: blood samples were collected from a single submandibular vein bleed from an individual mouse at different ages. 100 μ l of blood was collected into EDTA-treated Vacutainer tubes (BD) and used for whole blood cell counts. Another 100 μ l of blood was collected

into LiCl-treated plasma separator tubes; plasma was purified by centrifugation at 5000g for 5 min and used for blood biochemistry analysis.

Creating Physiological Frailty Index (PFI)

To quantitate the accumulation of health deficits PFI was created for each individual mouse as previously described²⁸. For this, we used 17 parameters that showed statistically significant age-dependent changes in control group of C57BL/6 male mice. These include: two physical parameters (body weight and grip strength), six hemodynamic parameters (systolic, diastolic and mean blood pressure, heart rate, tail blood flow, tail blood volume), total blood cell composition (white and red blood cell counts and differentials, nine total). Data are expressed as mean \pm SEM. Statistical analysis was performed using one or two-way ANOVA with Turkey post hoc test or t-test where appropriate. P-values <0.05 were considered significant.

Isolation and cultivation of adult primary mouse lung cells

Primary cell cultures were established with cells isolated from lung of TBI^{BMT} C57BL/6 mice and non-irradiated age matched control. Briefly, tissues were finely minced and incubated in DMEM media containing 2mg/ml dispase (Roche) at 4°C for 1 hour in a 50ml Falcon tube. The mixture was then mechanically dissociated and placed at 37°C for 30min. This step was repeated twice more, each time adding 2mg/ml of freshly prepared dispase enzyme. Up to 50ml of DMEM was added to the tube before centrifugation at 10,000rpm for 5 minutes. The supernatant was removed, and cells were plated in DMEM supplemented with 10% FBS and 50 μ g/ml penicillin/streptomycin.

Isolation and cultivation of adult mouse liver cells

Hepatocytes were isolated from TBI^{BMT} and non-irradiated adult C57BL/6 mice as described in (Gleiberman et al.) with slight modifications. Briefly, livers of anesthetized mice were perfused through the inferior vena cava. First perfusion was with EGTA (0.5 mM EGTA (Sigma) in PBS without calcium and magnesium) 30 ml total at a flow rate of 3-4 ml per minute (driven by a peristaltic pump). Following EGTA, livers were perfused with collagenase (0.02 % collagenase (Sigma) in DMEM with penicillin/streptomycin (50 ml). After collagenase perfusion, the gall bladder was removed, the liver excised from the animal and mechanically dispersed in 50 ml of DMEM media. Cells were then filtered through a 70 μ m-mesh and left to settle for 20 min on ice. The cell pellet was then re-suspended in 20 ml of DMEM, half of the suspension was carefully added to a double Percoll (Fisher Scientific) gradient (50% and 25% Percoll in PBS 20 ml each, 40 total) in a 50 ml conical tube. After 20 min centrifugation (1750xg) live hepatocytes from the bottom lowest fraction were re-suspended in 50 ml DMEM plus 10% FCS. Average yield of 30-

50x10⁶ nuclei per liver with 93-97% viability. Cells were then given 1.5 hours to attach in DMEM media, after which cells were washed in PBS and media replaced with William's E medium (WEM) (Invitrogen) containing 10% FCS and supplemented with penicillin/streptomycin, 2 mM glutamin (Invitrogen), 10 mM nicotinamide (Sigma), ITS (Sigma), 50 nm/ml EGF (Peprotech) and 10⁻⁷M dexamethasone (Sigma).

Cell cycle assay

Isolated lung cells were fixed in 70% precooled ethanol at 4°C for 12 hours. The fixed cells were washed with cold PBS and stained with propidium iodide (PI, 50ug/ml), RNase A (100µg/ml) and 0.2% Triton-X for 30min at 4°C in the dark. The stained cells were analyzed by flow cytometer.

Analysis of luminescence in p16^{INK4a}-luciferase mice

Mice were injected intraperitoneally with a 100 µl solution of 30 mg/mL D-luciferin potassium salt (Syd Labs) in D-PBS without calcium and magnesium. At 5 minutes post-injection, isoflurane-anesthetized mice were placed into the IVIS Spectrum *in vivo* bioluminescent imaging system (PerkinElmer) for detection of luciferase activity (60-second exposure). Bioluminescence in p16^{LUC} mice was quantified as total flux (p/s) of luminescent signal from the abdomen using via Living Image® software.

Mouse cytokine array

A cytokine array using a total of 30 cytokines and chemokines (RayBio) was used to examine pooled mouse serum collected from TBI^{BMT} and non-irradiated control C57Bl/6 mice 5 hours after the treatment with 10 µg/mouse of liposaccharide (LPS, Sigma). Mouse total blood was collected on heparin-based tubes via cardiac puncture. Serum was separated and mouse cytokine array was performed based on manufacturer's instructions.

Microarray analysis

Total RNA was extracted using Trizol (Invitrogen) from lung tissue of non-irradiated mice at 32 weeks of age, 78 weeks of age and TBI^{BMT} at 32 weeks of age. The resulting RNA samples were analyzed on Illumina Mouse WG-6 v2.0 Expression BeadChips containing probes for more than 45,200 transcripts by the Gene Expression Facility at Roswell Park Cancer Institute (Buffalo, NY).

Histological analysis of murine tissues

Tissue samples from TBI^{BMT} and age-matched non-irradiated C57BL/6 mice were collected and fixed in 10% neutral buffered formalin (Sigma). After paraffin embedding, tissues were sectioned

at 3 μm , and stained with hematoxylin and eosin to define morphology of each organ. General histological analysis was performed at $n=5$ for each group for each organ by light microscopy.

Immunoblotting

Proteins were extracted from cells using RIPA lysis buffer (Sigma-Aldrich). A total of 30 μg of total protein were loaded for electrophoresis into 4–12% Bis-Tris protein gels (Invitrogen). Proteins were transferred to a polyvinylidene difluoride membrane (Bio-Rad). Membranes were blocked with 5% milk in tris-buffered saline (TBS) with 0.1% Tween 20. Protein levels were detected using antibodies against phospho-histone H2A.X (Ser139) (Cell Signaling, #2577), anti-HMGB1 (Abcam, ab18256) and actin (BD Biosciences), followed by secondary horseradish-peroxidase conjugated antibodies. Bands were visualized using enhanced chemiluminescence (ECL) Plus western blotting detection reagents (Thermo Scientific).

EdU analysis of murine intestine

To label proliferating cells, a single intraperitoneal injection of thymidine analog 5-ethynyl-2'-deoxyuridine (EdU) (ThermoFisher) (50 mg/kg) 2 hours prior to tissue harvesting was administered to TBIBMT and age-matched non-irradiated C57Bl/6 mice. EdU incorporation into DNA was detected using the Click-iT EdU Alexa 488 Fluor Imaging kit (ThermoFisher) and counterstained with DAPI (Life Technologies) following manufacturer's instructions. Samples were examined using a Zeiss AxioImager A1 microscope equipped with an epifluorescent light source; images were captured with an AxioCam MRc digital camera and processed with a Zeiss Axio Imager Z1 microscope (Carl Zeiss, Germany)

EdU analysis of in vitro culture

Primary lung fibroblasts isolated from TBI^{BMT} and non-irradiated mice were labeled with EdU 8 and 72 hours after plating following manufacturer's instructions (ThermoFisher). Proportion of proliferating cells was calculated based on the ratio of EdU positive cells versus total number of cells present as indicated by DAPI staining.

Cell growth analysis

To determine cell growth, cells were plated in triplicate in 96-well plates at a density of 3,000 cells per well. At the indicated time, cells were fixed and stained using 0.4% methylene blue (USB) in 50% methanol (BDH). Plates were photographed or the dye was extracted from stained cells using 3% HCl solution for spectrophotometric quantitation.

FACS based cytokine analysis

Primary lung culture isolated from TBI^{BMT} and age-matched non-irradiated control were plated in 48-well format at 25,000 cells per well. Seventy-two hours after plating culture supernatants were collected. Levels of 3 cytokines (IL-6, CXCL1/KC, and G-CSF) were measured in the prepared supernatants in triplicate using mouse IL6, CXCL1/KC and G-CSF bead-based FlowCytomix kits (EBioscience Inc) according to the manufacturer's instructions. Cytokine levels were normalized to cell number of each condition.

Senescence-associated beta-galactosidase staining

Protocol was modified from Dimri et al. Cells were fixed with G/F fixative (0.8% Glutaraldehyde; 13.5% Formaldehyde; PBS). Then they were stained in SA- β -galactosidase solution (40mM Citric acid/Sodium phosphate buffer pH 6.0; 5mM Potassium Ferricyanide (Sigma); 5mM Potassium Ferrocyanide (Sigma); 2mM MgCl₂ (Sigma); 150mM NaCl (Sigma); 1mg/ml X-Gal (Invitrogen) dissolved in DMFA (Sigma). Staining was performed overnight at 37°C in the dark.

Immuno-fluorescent staining of DNA damage response

Primary lung fibroblasts were isolated as previously described from TBI^{BMT} and age-matched non-irradiated C57BL/6. The cells were fixed with 3% paraformaldehyde (Sigma) and 0.5% Triton X-100 (Sigma) in PBS for 10 minutes. The permeabilization was done in 0.5% Triton X-100 (Sigma) in PBS for 5 minutes and blocking was done in 3% bovine serum albumin (Sigma) for 30 minutes at room temperature. The cells were stained with following primary antibodies overnight at 4°C: 53BP1 (Cell Signaling, 1:500), phospho-RPA S4/8 (Bethyl; 1:500), XRCC1 (Abcam; 1:500) and γ -H2AX (Abcam; 1:500). Secondary antibodies used were AlexaFluor488 and AlexaFluor 555 (Invitrogen; 1:500) for 1 hour at room temperature. The cells were mounted with coverslips using ProLong™ Gold Antifade Mountant with DAPI (ThermoFisher), pictures were obtained with Zeiss 710 confocal microscope.

TUNEL assay

Was performed on de-paraffinized tissue sections using TdT In Situ Apoptosis Detection Kit – Fluorescein (R&D Systems) according to the manufacture instructions.

Imject-Alum granuloma formation assay

For the formation of the granuloma by injection of Alum (Thermo Scientific, Imject Alum), a subcutaneous injection of 800 mg/mouse of aluminum hydroxide on the dorsal side of the animal

was done. Thirteen days after the injection mice were euthanized and the granuloma was extracted and placed in NEG50 (ThermoFisher) in 2-methylbutane with dry ice.

Induction of skin wound

Full-thickness excisional wounds were prepared on shaved dorsal skin by 6-mm-punch biopsy. After wounding, each mouse was housed in a sterilized caged and was given 100 μ L of 0.01 mg/ml of buprenorphine at any signs of distress to minimize pain. Wound areas (width/length) were measured every day. Mice were sacrificed at various time points during healing or at the time of when the wound appeared completely healed (endpoint) for histological analysis.

Histological and immuno-histochemical analysis of skin wounds

Dissected skin samples were embedded into Neg-50 freezing medium and were fresh-frozen in slurry of dry ice-methyl butane. Cryosections 12 μ m thick immediately before staining were dried and fixed in 4% formaldehyde/PBS 5 min at room temperature, washed 3 times with PBS, incubated 15 min at room temperature with block solution (5% normal donkey serum, 0.25% triton x-100, PBS) and stained with cocktail of antibodies diluted in block solution: rat monoclonal anti-F4/80 antibody conjugated with AlexaFluor488 (BioLegend, 1:50 dilution); mouse monoclonal antibody against smooth muscle actin conjugated with Cy3 (SMA, Sigma, 1:500 dilution) and mouse monoclonal antibody against Ki67 conjugated with AlexaFluor647 (BD Pharmingen, 1:50 dilution). Slides were mounted with ProLong Diamond anti-fade reagent with DAPI (Invitrogen). The stained sections were analyzed using an AxioImager Z1 (Carl Zeiss Inc.) microscope equipped with epi-fluorescence and AxioCam HRc digital camera. Images were captured and processed with AxioVision software (release 4.5.3).

Tumor growth in vivo

Male C57Bl/6 mice (8-10 weeks of age were purchased from Jackson Lab). Half the mice were irradiated and rescued with bone marrow transplantation as described above. The C57Bl/6 mice were subcutaneously injected with 1.5×10^5 of B16-F10 cells in 100 μ L of PBS. Tumor volumes were measured every other day using a dial caliper. A group of mice was sacrificed and the tumors were dissected for H&E staining.

Supplementary Files

This is a list of supplementary files associated with this preprint. Click to download.

- [SupplementaryMaterial.pdf](#)